

Orbital-transverse density-wave instabilities in iron-based superconductors

Zi-Jian Yao,¹ Jian-Xin Li,² Q. Han,^{3,1} and Z. D. Wang¹

¹*Department of Physics and Center of Theoretical and Computational Physics,
The University of Hong Kong, Pokfulam Road, Hong Kong, China*

²*National Laboratory of Solid State Microstructures and Department of Physics, Nanjing University, Nanjing 210093, China*

³*Department of Physics, Renmin University of China, Beijing, China*

(Dated: February 4, 2022)

Besides the conventional spin-density-wave (SDW) state, a new kind of orbital-transverse density-wave (OTDW) state is shown to exist generally in multi-orbital systems. We demonstrate that the orbital character of Fermi surface nesting plays an important role in density responses. The relationship between antiferromagnetism and structural phase transition in LaFeAsO (1111) and BaFe₂As₂ (122) compounds of iron-based superconductors may be understood in terms of the interplay between the SDW and OTDW with a five-orbital Hamiltonian. We propose that the essential difference between 1111 and 122 compounds is crucially determined by the presence of the two-dimensional d_{xy} -like Fermi surface around (0,0) being only in 1111 parent compounds.

PACS numbers: 75.25.Dk, 75.30.Fv, 74.70.Kn

I. INTRODUCTION

Over the last two years, research on iron-based superconductors has been an exciting topic that attracts intensely experimental [1–5] and theoretical [6–11] investigations. Although it has been well established experimentally that this family of compounds exhibit several phase transitions including the structural phase transition [12–14], the antiferromagnetic (AF) phase transition [13–15], and the superconducting phase transition, the mechanism of these phase transitions remains highly controversial. However, there has been a consensus on the basic Fermi surface (FS) topology - hole pockets centered at (0, 0) and electron pockets centered at (π, π) [16–18]. From a viewpoint of itinerant antiferromagnetism, the hole and electron pockets are assumed to be nested nearly perfectly in the parent compound. The spin-density wave (SDW) state is stabilized due to the existence of the on-site Coulomb repulsions. Upon doping, the long range AF order is destroyed and short range AF spin fluctuations are developed, which is responsible for the high-temperature superconductivity [19, 20].

The multi-orbital nature of iron-based superconductors is believed to play a prominent role in the superconductivity, which signifies the importance of extracting the distinct physics that emerges from multi-orbital effects in this new family of materials. In this paper, we reveal that a new kind of unconventional orbital-transverse density-wave state exists generally in multi-orbital systems with certain orbital configuration of FS nesting. This type of density wave stems from the rotation asymmetry of Hamiltonian in the orbital space, which is reflected in the multi-orbital FS nesting geometry, and has an intriguing impact on the electron charge and spin density responses. In connection to the iron-based superconductors, our calculations show that the orbital-transverse density wave is a competing order with conventional SDW.

This paper is organized as follows. In Section II, we first consider three prototypes of FS nesting in the

multi-orbital systems. Then we define the density operators with two orbital degrees of freedom, and show how their responses are affected by the orbital configuration of FS nesting. In Section III, we show that the orbital-transverse density wave is nearly degenerated with the SDW by using a realistic five-orbital Hamiltonian of the iron-based superconductors. The interplay between the structure distortion and antiferromagnetism is discussed in the context of competing density-wave ground states. Finally, several remarks are drawn as the summary in Section IV.

II. DENSITY WAVES WITH ORBITAL DEGREES OF FREEDOM

A. Multi-orbital Hamiltonian

A multi-orbital Hamiltonian incorporating the on-site intra- and inter-orbital Coulomb interaction reads

$$H = H_0 + \frac{1}{2}U \sum_{i\alpha\sigma} n_{i\alpha\sigma} n_{i\alpha\bar{\sigma}} + \frac{1}{2}U' \sum_{i,\alpha\neq\beta} n_{i\alpha} n_{i\beta}, \quad (1)$$

where $H_0 = \sum_{i\alpha j\beta\sigma} t_{i\alpha,j\beta} c_{i\alpha\sigma}^\dagger c_{j\beta\sigma}$, $t_{i\alpha,j\beta}$ is the hopping term between orbital α of site i and orbital β of site j , and $n_{i\alpha\sigma}$ the electron number operator, U and U' is the on-site intra- and inter-orbital Coulomb repulsion, respectively. For simplicity, U is assumed to be equal to U' in the present study and the terms of Hund's rule coupling are ignored. In order to illustrate various types of density responses of the multi-orbital system more clearly, we start from a simple two-orbital model in the square lattice with a hole pocket lying at (0, 0) and an electron pocket lying at $(\pi, 0)$. The dispersion and chemical potential ensure that the electron pocket and hole pocket are circular and nested perfectly. This fermiology is compatible with many possible orbital configurations, which have different orbital-weights of the FS. In Fig. 1 we

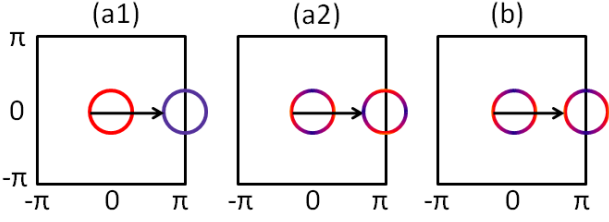


FIG. 1: (Color online) Schematic plot of the Fermi surfaces with different orbital configurations. Blue and red indicate dominant weights of orbital 1 and 2, respectively.

show three prototypes of them. As will see below, the density response behaviors of them are quite different.

B. Definition of density quantities

The introduction of orbital degrees of freedom enables us to define extra physical quantities of density whose translational symmetry could be broken when the system is phase transferred into the density-wave ground state. Similar to the spin- $\frac{1}{2}$ degrees of freedom, we represent the two-orbital degrees of freedom by an $\frac{1}{2}$ pseudospin. The density operators in such a spin-orbital space can be written as $\mathbf{D}(r_i) = \phi_i^\dagger \mathbf{\Gamma} \phi_i$ with $\mathbf{\Gamma} = \tau \otimes \sigma$ and $\phi_i^\dagger = [c_{i1\uparrow}^\dagger, c_{i1\downarrow}^\dagger, c_{i2\uparrow}^\dagger, c_{i2\downarrow}^\dagger]$ the 4-component spinor ($\tau^0 = \sigma^0 = \mathbb{I}$ and $\tau^{1-3} = \sigma^{1-3}$ the Pauli matrices, where τ is defined in the orbital space and σ is defined in the spin space). To study the instability in the particle-hole channels, the sixteen particle-hole operators $\phi^\dagger (\tau^{0-3} \otimes \sigma^{0-3}) \phi$ can be reduced into six different density channels (three of spin and three of charge) due to the SU(2) symmetry of Hamiltonian (1) in the spin space, which are listed in Table I.

The six channels listed in Table I could be further grouped into four types of density waves, if we are not interested in the direction of the density orbital-polarization, namely the total spin-density wave, the total charge-density wave, the orbital-polarized spin-density wave, and the orbital-polarized charge-density wave. Basically the orbital-polarized density operator represents the difference of density between two orthogonal orbitals. The longitudinal or transverse polarization of orbital determines which two orthogonal orbitals are density-ordered, for instance, the longitudinal polarization corresponds to a density-ordered state between orbital 1 and 2 while the transverse polarization corresponds to a density-ordered state between two orthogonal mixtures of orbitals 1 and 2. The distinction between orbital-longitudinal and orbital-transverse parts of the susceptibilities is consequent to the rotation asymmetry of the Hamiltonian (1) in the orbital space. In Fig. 2 we plot schematically the ground states of these density-wave states in real space.

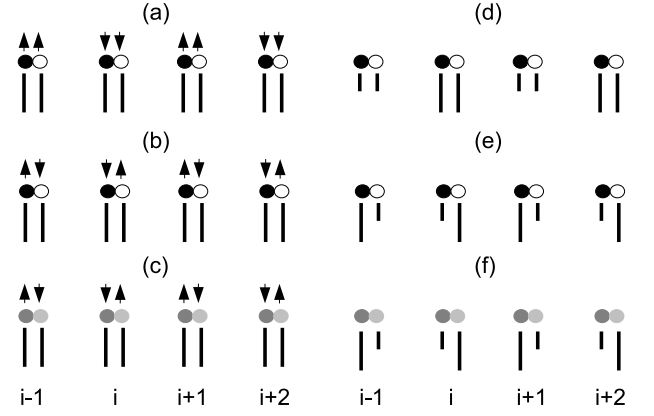


FIG. 2: Schematic plot of density waves with wave vector $Q = (\pi, 0)$, (a)-(f) correspond to the density-wave states with density operators $D_{0,3}$, $D_{3,3}$, $D_{-(+),3}$, $D_{0,0}$, $D_{3,0}$, and $D_{-(+),0}$. Black (blank) circle represents orbital 1 (2). Dark grey and grey circles represent two orthogonal mixtures of orbitals 1 and 2, e.g., $\frac{1}{\sqrt{2}}(|1\rangle + |2\rangle)$ for dark grey and $\frac{1}{\sqrt{2}}(|1\rangle - |2\rangle)$ for grey. The arrow indicates spin density and the vertical line indicates the charge density. $i, i+1, \dots$ denote the lattice sites and each site represents a reduced unit cell. Only modulated direction is shown.

C. Instability criterions

The particle-hole instabilities in the presence of Coulomb interactions may be examined within the random-phase approximation (RPA). The interaction matrices for the magnetic (\hat{U}^s) and charge (\hat{U}^c) channels reads

$$\hat{U}^s = \begin{pmatrix} \hat{U}^{s1} & 0 \\ 0 & \hat{U}^{s2} \end{pmatrix}, \hat{U}^c = \begin{pmatrix} \hat{U}^{c1} & 0 \\ 0 & \hat{U}^{c2} \end{pmatrix}, \quad (2)$$

where $\hat{U}^{s1} = \text{diag}(U, U)$, $\hat{U}_{mn}^{c1} = U$ for $m = n$ and $2U'$ otherwise, $\hat{U}^{s2} = \text{diag}(U', U') = -\hat{U}^{c2}$. Defining the orbital indices of the bare susceptibility as $\chi_{\alpha\beta\mu\nu}^0(q) = -\frac{T}{N} \sum_k G_{\alpha\mu}^0(k+q) G_{\nu\beta}^0(k)$, we get the RPA spin and charge susceptibility matrices

$$\begin{aligned} \hat{\chi}^s(q) &= [\hat{I} - \hat{\chi}^0(q) \hat{U}^s]^{-1} \hat{\chi}^0(q), \\ \hat{\chi}^c(q) &= [\hat{I} + \hat{\chi}^0(q) \hat{U}^c]^{-1} \hat{\chi}^0(q). \end{aligned} \quad (3)$$

The response functions listed in Table I are given by

$$\begin{aligned} \tilde{\chi}_{A,B}(q, i\omega) &= \frac{1}{2} \int_0^\beta d\tau e^{i\omega\tau} \langle T_\tau D_{A,B}(q, \tau) D_{A,B}(-q, 0) \rangle \\ \tilde{\chi}_{-,B}(q, i\omega) &= \frac{1}{2} \int_0^\beta d\tau e^{i\omega\tau} \langle T_\tau D_{-,B}(q, \tau) D_{+,B}(-q, 0) \rangle \end{aligned} \quad (4)$$

where A and B are numbers and $D_{A,B} = \phi^\dagger (\tau_A \otimes \sigma_B) \phi$. A direct calculation gives the response functions of density

TABLE I: Density waves with two orbital degrees of freedom

Ordering type of densities	Orientation in orbital space	Density operator	Response function	Divergent blocks
total spin	n/a	$D_{0,3}(r_i): \rho_{i1\uparrow} - \rho_{i1\downarrow} + \rho_{i2\uparrow} - \rho_{i2\downarrow}$	$\frac{1}{2}(\chi_{1111}^s + \chi_{2222}^s + \chi_{1122}^s + \chi_{2211}^s)$	$\hat{\chi}^{s1}$
total charge	n/a	$D_{0,0}(r_i): \rho_{i1\uparrow} + \rho_{i1\downarrow} + \rho_{i2\uparrow} + \rho_{i2\downarrow}$	$\frac{1}{2}(\chi_{1111}^c + \chi_{2222}^c + \chi_{1122}^c + \chi_{2211}^c)$	$\hat{\chi}^{c1}$
orbital- polarized spin	longitudinal	$D_{3,3}(r_i): \rho_{i1\uparrow} - \rho_{i1\downarrow} - (\rho_{i2\uparrow} - \rho_{i2\downarrow})$	$\frac{1}{2}(\chi_{1111}^s + \chi_{2222}^s - \chi_{1122}^s - \chi_{2211}^s)$	$\hat{\chi}^{s1}$
	transverse	$D_{-(+),3}(r_i): c_{i2\uparrow}^\dagger c_{i1\uparrow} - c_{i2\downarrow}^\dagger c_{i1\downarrow} \text{ (H.c.)}$	χ_{2121}^s	$\hat{\chi}^{s2}$
orbital- polarized charge	longitudinal	$D_{3,0}(r_i): \rho_{i1\uparrow} + \rho_{i1\downarrow} - (\rho_{i2\uparrow} + \rho_{i2\downarrow})$	$\frac{1}{2}(\chi_{1111}^c + \chi_{2222}^c - \chi_{1122}^c - \chi_{2211}^c)$	$\hat{\chi}^{c1}$
	transverse	$D_{-(+),0}(r_i): c_{i2\uparrow}^\dagger c_{i1\uparrow} + c_{i2\downarrow}^\dagger c_{i1\downarrow} \text{ (H.c.)}$	χ_{2121}^c	$\hat{\chi}^{c2}$

operators defined in Table I

$$\begin{aligned}
\tilde{\chi}_{0,3} &= \frac{1}{2}(\chi_{1111}^s + \chi_{2222}^s + \chi_{1122}^s + \chi_{2211}^s), \\
\tilde{\chi}_{0,0} &= \frac{1}{2}(\chi_{1111}^c + \chi_{2222}^c + \chi_{1122}^c + \chi_{2211}^c), \\
\tilde{\chi}_{3,3} &= \frac{1}{2}(\chi_{1111}^s + \chi_{2222}^s - \chi_{1122}^s - \chi_{2211}^s), \\
\tilde{\chi}_{-,+,3} &= \chi_{2121}^s, \\
\tilde{\chi}_{3,0} &= \frac{1}{2}(\chi_{1111}^c + \chi_{2222}^c - \chi_{1122}^c - \chi_{2211}^c), \\
\tilde{\chi}_{-,+,0} &= \chi_{2121}^c.
\end{aligned} \tag{5}$$

To a good approximation, especially at $Q = (\pi, 0)$, the bare susceptibility matrix in the two-orbital case can be regarded as a block matrix $\hat{\chi}^0 = \text{diag}(\hat{\chi}^1, \hat{\chi}^2)$, where

$$\hat{\chi}^1 = \begin{pmatrix} \chi_{1111}^0 & \chi_{1122}^0 \\ \chi_{2211}^0 & \chi_{2222}^0 \end{pmatrix}, \hat{\chi}^2 = \begin{pmatrix} \chi_{1212}^0 & \chi_{1221}^0 \\ \chi_{2112}^0 & \chi_{2121}^0 \end{pmatrix}.$$

As a result, the RPA spin and charge susceptibility matrices are also blocked,

$$\hat{\chi}^{s(c)} = \begin{pmatrix} \hat{\chi}^{s1(c1)} & 0 \\ 0 & \hat{\chi}^{s2(c2)} \end{pmatrix}, \tag{6}$$

where

$$\hat{\chi}^{s1} = \frac{\hat{M}_1}{d_1}, \hat{\chi}^{s2} = \frac{\hat{M}_2}{d_2}, \hat{\chi}^{c1} = \frac{\hat{M}_3}{d_3}, \hat{\chi}^{c2} = \frac{\hat{M}_4}{d_4}. \tag{7}$$

Here M_n are some 2×2 matrices and

$$\begin{aligned}
d_1 &= \det[\hat{\chi}^{s1}] = (1 - U\chi_{1111}^0)(1 - U\chi_{2222}^0) - U^2\chi_{1122}^0\chi_{2211}^0, \\
d_2 &= \det[\hat{\chi}^{s2}] = (1 - U'\chi_{1212}^0)(1 - U'\chi_{2121}^0) - U'^2\chi_{1221}^0\chi_{2112}^0, \\
d_3 &= \det[\hat{\chi}^{c1}] = 1 + U(\chi_{1111}^0 + \chi_{2222}^0) + 2U'(\chi_{1122}^0 + 2\chi_{2211}^0) \\
&\quad + (U^2 - 4U'^2)(\chi_{1111}^0\chi_{2222}^0 - \chi_{1122}^0\chi_{2211}^0) \\
d_4 &= d_2
\end{aligned} \tag{8}$$

are the denominators that come from the inversion of matrices $\hat{I} - \chi^0(q)\hat{U}^s$ and $\hat{I} + \chi^0(q)\hat{U}^c$ in Eq. (7). Deviated from the single band RPA, there are two instability criterions for the spin channel, which are indicated by $d_1 \rightarrow 0$ and $d_2 \rightarrow 0$, respectively. When approaching the critical temperature, either the upper block χ^{s1} or the

lower block χ^{s2} may diverge. Comparing the response functions listed in Table I and Eq. (7), we can see that the divergence of the upper block or the lower block corresponds to a transition to one or the other totally different magnetic phase, i.e., the former indicates an SDW transition while the latter indicates an orbital-transverse polarized spin-density-wave transition. The same conclusion holds for the charge susceptibility matrix. We will refer the orbital-transverse density-wave ground state as OTDW in this paper hereafter.

Now we turn to the real-space distribution of these density waves. As discussed in Section II B, it is clear that the orbital-longitudinal operators represent the density differences between orbitals 1 and 2. On the other hand, the real-space distribution of the orbital-transverse density wave can be revealed by performing a rotation in the orbital space:

$$\psi_i^\dagger = [c_{i+\uparrow}^\dagger, c_{i+\downarrow}^\dagger, c_{i-\uparrow}^\dagger, c_{i-\downarrow}^\dagger],$$

where

$$c_{i\pm\sigma}^\dagger = \frac{1}{\sqrt{2}}(c_{i1\sigma}^\dagger \pm c_{i2\sigma}^\dagger).$$

The charge and spin density differences between the two orbitals $|+\rangle$ and $|-\rangle$ can be represented by

$$\begin{aligned}
D'_{3,3}(r_i) &= \psi_i^\dagger(\tau_3 \otimes \sigma_3)\psi = S_{i+,z} - S_{i-,z} \\
&= c_{i1\uparrow}^\dagger c_{i2\uparrow} - c_{i1\downarrow}^\dagger c_{i2\downarrow} + \text{H.c.}, \\
D'_{3,0}(r_i) &= \psi_i^\dagger(\tau_3 \otimes \sigma_0)\psi = \rho_{i+} - \rho_{i-} \\
&= c_{i1\uparrow}^\dagger c_{i2\uparrow} + c_{i1\downarrow}^\dagger c_{i2\downarrow} + \text{H.c.},
\end{aligned}$$

where $S_{i\pm,z}$ and $\rho_{i\pm}$ represent the spin and charge density of orbital $|\pm\rangle$ at i site, respectively. Similarly, the response functions for density operators $D'_{A,B}$ are

$$\begin{aligned}
\tilde{\chi}'_{3,3} &= \frac{1}{2}(\chi_{1212}^s + \chi_{2121}^s + \chi_{1221}^s + \chi_{2112}^s), \\
\tilde{\chi}'_{3,0} &= \frac{1}{2}(\chi_{1212}^c + \chi_{2121}^c + \chi_{1221}^c + \chi_{2112}^c).
\end{aligned} \tag{9}$$

Therefore, in OTDW state, the translational symmetry of the local density difference between the two orthogonal mixtures of orbitals 1 and 2 is broken.

D. Nesting-induced OTDW: a weak-coupling analysis

Roughly speaking, the density response of a Hubbard-like Hamiltonian is mainly determined by two factors: one is the band structure, and the other is the Coulomb interactions. We now look into the influence of different band structures shown in Fig. 1 on the density responses. The bare susceptibility of a general multi-orbital system is given by

$$\chi_{\alpha\beta\mu\nu}^0(q, 0) = \frac{1}{N} \sum_{k, mn} a_m^{\alpha*}(k+q) a_n^\beta(k) a_n^{\nu*}(k) a_m^\mu(k+q) \frac{f[\epsilon_n(k+q)] - f[\epsilon_m(k)]}{\epsilon_m(k) - \epsilon_n(k+q) + i\eta}, \quad (10)$$

where α, β, μ and ν are the orbital indices, m and n are the band indices, and a is the orbital weight. For the case indicated in Fig. 1 (a1), the matrix elements of bare susceptibility are simplified to

$$\chi_{\mu\nu\mu\nu}^0(q, 0) = \frac{1}{N} \sum_{k, \mu\nu} \frac{f[\epsilon_\nu(k+q)] - f[\epsilon_\mu(k)]}{\epsilon_\mu(k) - \epsilon_\nu(k+q) + i\eta}. \quad (11)$$

The susceptibilities $\chi_{\mu\mu\nu\nu}^0$ ($\mu \neq \nu$) vanish since there is no hybridization between the two orbitals. Straightforwardly, $\chi_{1212}^0(Q)$ and $\chi_{2121}^0(Q)$ are divergent due to FS nesting, while χ_{1111}^0 and χ_{2222}^0 keep finite as they take no advantage from the nesting between electron and hole pockets. Bear in mind that although the cases of Fig. 1 (a1) and (a2) have different orbital configurations, their FS nestings are both from the inter-orbital contribution [21]. Hence the above conclusion holds also for the band structure shown in (a2). For the case Fig. 1 (b), from Eq. (10) the divergent components of bare susceptibilities are χ_{1111}^0 and χ_{2222}^0 .

The above considerations focus on the band structure, but do not take into account the electron-electron interactions explicitly. Given the interaction vertices in Eq. (2) and the instability criteria in Eq. (8), three spin-density waves ($D_{0,3}$, $D_{3,3}$, and $D_{-(+),3}$), and one charge-density wave ($D_{-(+),0}$) could be established in Hamiltonian (1). The $D_{0,0}$ and $D_{3,0}$ charge-density waves are prohibited due to repulsive on-site Coulomb interactions (note that d_3 is always greater than zero when $U\chi_{1111/2222}^0 < 1$ and the hybridization is neglectable). $D_{0,3}$ and $D_{3,3}$ density waves occur simultaneously since they both come from the divergent of the upper block of $\hat{\chi}^s(Q)$, which indicates the real-space distribution of spin density to be compatible with Fig. 2 (a) and (b). A typical pattern of spin density that is either $D_{0,3}$ or $D_{3,3}$ density wave is shown in Fig. 3, where the staggered spin density is orbital-polarized and dominantly appears in one orbital. On the other hand, the phase transition in $D_{-(+),0(3)}$ channel comes from the divergent of the lower block of $\hat{\chi}^{s(c)}(Q)$ which is coupled to the inter-orbital repulsion, with order parameter $\langle c_{\mu\sigma}^\dagger(k+Q)c_{\nu\bar{\sigma}(\sigma)}(k) \rangle$. In the present model,

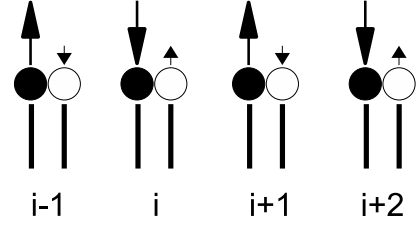


FIG. 3: Intra-orbital nesting induced spin-density-wave state that is realized in the iron-based superconductors, where the translational symmetries of $\langle D_{0,3} \rangle$ and $\langle D_{3,3} \rangle$ are broken simultaneously. All the symbols are the same as that in Fig. 2.

instabilities in $D_{-(+),3}$ and $D_{-(+),0}$ channels are degenerated due to $U = U'$, while the actually established state depends on the additional interaction terms that break the degeneracy, e.g., the former is favored by Hund's rule coupling while the latter is favored by the presence of electron-phonon interactions.

We now conclude that for configurations shown in Fig. 1 (a1) and (a2), the divergent susceptibility matrix is $\chi^{s2}(Q)$ or $\chi^{c2}(Q)$, indicating that the system undergoes an OTDW transition. There is no long range order of the total local spin density, as is shown in Fig. 2 (c) and (f). For configuration Fig. 1 (b), the divergent susceptibility matrix is $\chi^{s1}(Q)$, corresponding to a spin density-wave transition whose real-space distribution is shown in Fig. 3.

III. OTDW AND THE IRON-BASED SUPERCONDUCTORS

The multi-orbital band structure of iron-based superconductors provides an intermediate example between prototypes of Fig. 1 (a) and (b). To be more concrete, we here employ a realistic five-orbital Hamiltonian with on-site intra- and inter-orbital Coulomb repulsions. The involved orbitals are d_{xz} , d_{yz} , $d_{x^2-y^2}$, d_{xy} , and $d_{3z^2-r^2}$ (defined in the reduced unit cell) which are labeled with 1, 2, 3, 4, and 5 respectively. Then the orbital indices in Hamiltonian (1) run from 1 to 5. We adopt the hopping parameters given by Graser *et al* [22] fitted from first principle calculated band structure by Cao *et al* [23]. The density-wave instabilities defined in Table I can be realized in the space spanned by the two most relevant orbitals. In our calculations, d_{xz}/d_{yz} (orbital 1/2) and d_{xy} (orbital 4) are the two orbitals with largest intra- and inter-orbital susceptibilities. The instabilities of OTDW and SDW are found to be nearly degenerated, consequently the competition between them is sensitive to the detailed band structure. We consider this to be a key point to understand the essential difference between $R\text{FeAsO}$ (1111) and $A\text{Fe}_2\text{As}_2$ (122) compounds (R =rare earth and A =Sr, Ca, Ba and K), which will be discussed in the following paragraphs.

The AF and structural transitions in the iron-based superconductors exhibit different properties in different systems: the static AF order develops after the structure distortion in 1111 compounds [13], while in the 122 compounds, the two transitions occur at the same temperature [14, 24]. The structure distortion has been theoretically proposed to be driven magnetically [25–27] or electrically [28, 29]. Here we present an alternative view. Note that all the density waves we discuss are nesting-driven and occur at the same wave-vector $Q = (\pi, 0)$. The order parameters of these density waves and the tetragonal-to-orthorhombic distortion break the same symmetry. Therefore, we propose that either spin-polarized SDW (shown in Fig. 3) or OTDW could induce a structure distortion. When the transition temperature of SDW T_{d1} is higher than that of OTDW T_{d2} , the AF transition is orbital-polarized as shown in Fig. 3 and is accompanied with a structure distortion which is magnetically driven, and the critical temperature of structure distortion T_S and AF transition T_{AF} equal to T_{d1} . The temperature gap between T_S and T_{AF} appears when $T_{d2} > T_{d1}$, which indicates $T_S = T_{d2} > T_{AF} = T_{d1}$. We make two remarks here. First, $D_{-(+),0}$ and $D_{-(+),3}$ density waves are two candidates for OTDW-induced lattice distortion. As an orbital-ordered state of charge, $D_{-(+),0}$ density wave could induce a structure distortion electrically by Jahn-Teller effect. The coupling between $D_{-(+),0}$ density wave and lattice distortion is, if exists, magnetic relevant and more subtle. It is out of scope of the present work to determine which of the two density waves is *actually* established in the real materials of iron-based superconductors. Since the two states are degenerated in our model, we just generally related the structure distortion with OTDWs. Second, in this scenario, from high temperature to low temperature, the system undergoes two phase transitions, both couple to a structure distortion. However, only one structure distortion is identified in experimental measurements. We note the lattice distortion is weak and driven by breaking of C_4 lattice rotation symmetry. Thus if the system is already in the orthorhombic structure phase, another density-wave phase transition with wave-vector $(\pi, 0)$ would not break an extra lattice symmetry.

It is known from band calculations of 1111 compounds that along Γ -Z direction lies a d_{xy} -like two-dimensional (2D) FS (denoted as ε -FS hereafter) [30]. While for 122 compounds, a 2D FS with d_{xy} character is found to be absent when the pnictogen height is relaxed using total-energy minimization [31]. In our model calculation we find the existence of ε -FS enhances the inter-orbital susceptibility χ_{1414}^0 substantially, while without ε -FS, the susceptibility χ_{1111}^0 is in general, at least slightly, stronger than that of χ_{1414}^0 . The enhancement of χ_{1414}^0 by the appearance of a d_{xy} -like FS is expected because of the strengthened inter-orbital nesting between ε -FS and the d_{xz}/d_{yz} -dominant FS sections around M. In Fig. 4 we show dominant components (1111 and 1414) of spin susceptibility matrix with (upper) and without (lower) the appearance of ε -FS.

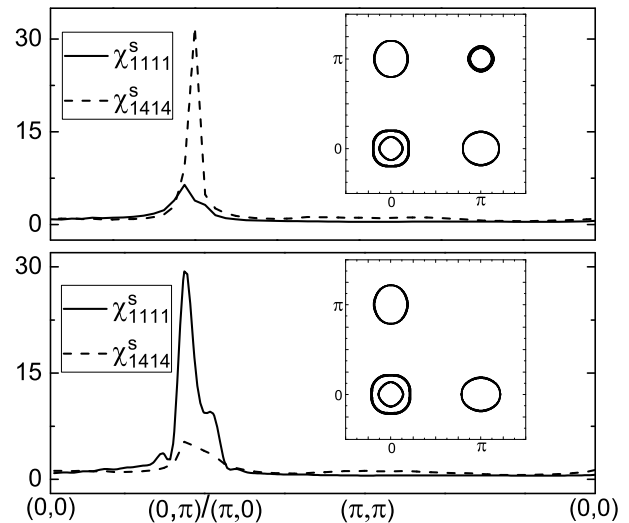


FIG. 4: Dominant components of spin susceptibility matrix with (upper) and without (lower) the appearance of ε -FS. The hopping parameters are adopted from [22], $U = U' = 1.38$ and $T = 0.19$ for the upper panel and $U = U' = 1.53$ and $T = 0.17$ for the lower panel. To produce the ε -FS, the on-site energy of orbital d_{xy} is adjusted from 0.3 to 0.38 and μ is adjusted to 0.006 in the upper panel. All energy quantities are in units of eV.

appearance of the ε -FS. To produce the ε -FS, the on-site energy of orbital d_{xy} is adjusted from 0.3 to 0.38, and μ is adjusted from 0 to 0.006 to keep the band filling at $n = 6$ in the upper panel, where the divergent susceptibility is χ_{1414}^s at $T = 0.019$ and $U = 1.38$. In the lower panel, χ_{1414}^s is suppressed by the annihilation of the ε -FS, and the divergent channel changes to χ_{1111}^s . With the definition of pseudo-transition-temperatures T_{d1}^* and T_{d2}^* as $\chi^s(Q, T_{d1(d2)}^*) = 10^2 \chi^0(Q, T_{d1(d2)}^*)$, our numerical results show that the transition temperature $T_{d2}^* = 0.019$ is higher than $T_{d1}^* = 0.012$ in the presence of ε -FS, which leads to a higher transition temperature of OTDW than that of SDW, thus the separation between T_S and T_N appears, as is observed in 1111 compounds. Without ε -FS, we get $T_{d1}^* = 0.017 > T_{d2}^* = 0.0068$ which indicates same T_S and T_N in our scenario, as is observed in 122 compounds. In this sense, the essential difference in the structure distortion between 1111 and 122 systems may be attributed to the existence of ε -FS in 1111 parent compounds. Meanwhile, we want to emphasize that depending on the detailed band structure, there are other possible realizations of OTDW, such as the inter-orbital nesting between d_{xz} and d_{yz} orbitals. The importance of the ε -FS in splitting T_S and T_N awaits for further experimental verification.

IV. SUMMARY

We make several remarks as the summary. (1) As has already been addressed, the OTDW is not a static or-

dered state of total charge or spin density, which makes it “invisible” to the neutron detections. (2) The transverse nature of OTDW implies that the ordered orbital component is a mixture of the two involved orbitals, for instance, a mixture of d_{xz}/d_{yz} and d_{xy} orbitals in the iron-based superconductors. (3) In our model calculations, the instabilities of OTDWs occur in the space spanned by d_{xz} (or d_{yz}) and d_{xy} orbitals. However, depending on the band structure, other possibilities exist. (4) The OTDW might be related with the “hidden” order claimed by some experiments [32]. (5) One intriguing feature stemming from the itinerant multi-orbital model is that

the established SDW should be orbital-polarized (as is shown in Fig. 3).

Acknowledgments

The work was supported by the RGC of Hong Kong under Grant No. HKU7055/09P, the URC fund of HKU, the NSFC (No. 10525415 and No. 10674179), and the 973 Program of China (No. 2006CB921800).

-
- [1] Y. Kamihara, T. Watanabe, M. Hirano, and H. Hosono, *Journal of the American Chemical Society* **130**, 3296 (2008).
 - [2] X. H. Chen, T. Wu, G. Wu, R. H. Liu, H. Chen, and D. F. Fang, *Nature* **453**, 761 (2008).
 - [3] Z.-A. Ren, J. Yang, W. Lu, W. Yi, X.-L. Shen, Z.-C. Li, G.-C. Che, X.-L. Dong, L.-L. Sun, F. Zhou, et al., *EPL (Europhysics Letters)* **82**, 57002 (2008).
 - [4] G. F. Chen, Z. Li, D. Wu, G. Li, W. Z. Hu, J. Dong, P. Zheng, J. L. Luo, and N. L. Wang, *Phys. Rev. Lett.* **100**, 247002 (2008).
 - [5] M. Rotter, M. Tegel, and D. Johrendt, *Phys. Rev. Lett.* **101**, 107006 (2008).
 - [6] Q. Han, Y. Chen, and Z. D. Wang, *EPL (Europhysics Letters)* **82**, 37007 (2008).
 - [7] M. Daghofer, A. Moreo, J. A. Riera, E. Arrigoni, D. J. Scalapino, and E. Dagotto, *Phys. Rev. Lett.* **101**, 237004 (2008).
 - [8] W.-Q. Chen, K.-Y. Yang, Y. Zhou, and F.-C. Zhang, *Phys. Rev. Lett.* **102**, 047006 (2009).
 - [9] V. Cvetkovic and Z. Tesanovic, *Phys. Rev. B* **80**, 024512 (2009).
 - [10] A. V. Chubukov, D. V. Efremov, and I. Eremin, *Phys. Rev. B* **78**, 134512 (2008).
 - [11] S.-L. Yu, J. Kang, and J.-X. Li, *Phys. Rev. B* **79**, 064517 (2009).
 - [12] J. Zhao, Q. Huang, C. de la Cruz, L. Shiliang, J. W. Lynn, Y. Chen, M. A. Green, G. F. Chen, G. Li, Z. Li, et al., *Nat Mater* **7**, 953 (2008).
 - [13] M. A. McGuire, A. D. Christianson, A. S. Sefat, B. C. Sales, M. D. Lumsden, R. Jin, E. A. Payzant, D. Mandrus, Y. Luan, V. Keppens, et al., *Phys. Rev. B* **78**, 094517 (2008).
 - [14] C. Krellner, N. Caroca-Canales, A. Jesche, H. Rosner, A. Ormeci, and C. Geibel, *Phys. Rev. B* **78**, 100504 (2008).
 - [15] J. Dong, H. J. Zhang, G. Xu, Z. Li, G. Li, W. Z. Hu, D. Wu, G. F. Chen, X. Dai, J. L. Luo, et al., *EPL (Europhysics Letters)* **83**, 27006 (2008).
 - [16] H. Ding, P. Richard, K. Nakayama, K. Sugawara, T. Arakane, Y. Sekiba, A. Takayama, S. Souma, T. Sato, T. Takahashi, et al., *EPL (Europhysics Letters)* **83**, 47001 (2008).
 - [17] T. Sato, K. Nakayama, Y. Sekiba, P. Richard, Y.-M. Xu, S. Souma, T. Takahashi, G. F. Chen, J. L. Luo, N. L. Wang, et al., *Phys. Rev. Lett.* **103**, 047002 (2009).
 - [18] C. Liu, G. D. Samolyuk, Y. Lee, N. Ni, T. Kondo, A. F. Santander-Syro, S. L. Bud'ko, J. L. McChesney, E. Rotenberg, T. Valla, et al., *Phys. Rev. Lett.* **101**, 177005 (2008).
 - [19] Z.-J. Yao, J.-X. Li, and Z. D. Wang, *New Journal of Physics* **11**, 025009 (2009).
 - [20] F. Wang, H. Zhai, Y. Ran, A. Vishwanath, and D.-H. Lee, *Phys. Rev. Lett.* **102**, 047005 (2009).
 - [21] The hybridization parts of Fig. 1 (a2) and (b) are assumed to be neglecting small, so we can safely ignore the off-diagonal blocks of the susceptibility matrices.
 - [22] S. Graser, T. A. Maier, P. J. Hirschfeld, and D. J. Scalapino, *New Journal of Physics* **11**, 025016 (2009).
 - [23] C. Cao, P. J. Hirschfeld, and H. Cheng, *Phys. Rev. B* **77**, 220506 (2008).
 - [24] J. Zhao, W. Ratcliff, II, J. W. Lynn, G. F. Chen, J. L. Luo, N. L. Wang, J. Hu, and P. Dai, *Phys. Rev. B* **78**, 140504 (2008).
 - [25] T. Yildirim, *Phys. Rev. Lett.* **101**, 057010 (2008).
 - [26] C. Fang, H. Yao, W.-F. Tsai, J. Hu, and S. A. Kivelson, *Phys. Rev. B* **77**, 224509 (2008).
 - [27] C. Xu, M. Müller, and S. Sachdev, *Phys. Rev. B* **78**, 020501 (2008).
 - [28] A. M. Turner, F. Wang, and A. Vishwanath (2009), arXiv:0905.3782.
 - [29] W. Lv, J. Wu, and P. Phillips, *Phys. Rev. B* **80**, 224506 (2009).
 - [30] V. Vildosola, L. Pourovskii, R. Arita, S. Biermann, and A. Georges, *Phys. Rev. B* **78**, 064518 (2008).
 - [31] D. J. Singh, *Phys. Rev. B* **78**, 094511 (2008).
 - [32] V. B. Zabolotnyy, D. S. Inosov, D. V. Evtushinsky, A. Koitzsch, A. A. Kordyuk, G. L. Sun, J. T. Park, D. Haug, V. Hinkov, A. V. Boris, et al., *Nature* **457**, 569 (2009).